Energy xxx (2014) 1–9

Contents lists available at ScienceDirect

Energy

journal homepage: www.elsevier.com/locate/energy

Theoretical, experimental and numerical diagnose of critical power point of thermoelectric generators

Min Chen*, Xin Gao

Institute of Energy Technology, Aalborg University, Pontoppidanstraede 101, DK-9220 Aalborg, Denmark

ARTICLE INFO

Article history:
Received 17 June 2014
Received in revised form
30 September 2014
Accepted 6 October 2014
Available online xxx

Keywords:
Thermoelectric generator
Output power
Nonuniform temperature distribution
Hierarchical modeling
Critical power point
Series–parallel connection

ABSTRACT

When a number of TEMs (thermoelectric modules) are connected in a series–parallel matrix and under mismatched temperature gradients, the overall maximum output power of the thermoelectric generator (TEG) may be lowered by certain TEMs with relatively smaller temperature difference. It is possible to avoid such a performance decrease by the disconnection of these low temperature TEMs, provided that the critical power point can be accurately determined. In this paper, firstly a rigorous and universal formulation is fully detailed to mathematically determine the conceptions and conditions of the critical power point in the series and parallel TEM arrays. Secondly, experiments of a series–parallel hybrid interconnected TEG are presented to clearly quantify the theoretical analyses. Finally, the hierarchical simulation, based on the SPICE (simulation program with integrated circuit emphasis) platform, is applied to estimate the critical power point. By numerically modeling the nonlinear physical processes of the TEG, the simulation can be used as an enabling technique in any model-based controller to dynamically minimize the mismatch power loss within the TEM matrix of any configuration. In experimental and numerical results, a number of critical power points are disclosed for a 2×4 parallel–serial hybrid TEM matrix, where the hot temperature mostly ranges from 120 °C to 60 °C.

1. Introduction

TEGs (Semiconductor thermoelectric generators) have the merits of high durability, great environmental harmony, and pure DC (direct current) power source. As they can recover the huge amount of low grade waste heat into electricity in a simple manner, TEG systems have been of great interest to energy applications in recent years. Representative examples of TEGs include fuel fired combustors and thermal fluid tubes in industrial power plants and private sectors [1–7], as well as the exhaust pipes in fuel cells [8–11], aircrafts [12] and vehicles [13–19], where thermoelectric modules (TEMs) can be mounted on heat sources to operate as an array of thermal batteries that supplies power to the load.

In composing a battery pack, ordinary voltage sources such as alkaline batteries usually prefer the series connection. This is because, if the batteries are mismatched, then those with higher voltage may charge others when the batteries are connected in parallel. In this case, the batteries with lower voltage cannot work normally to output power and may be overheated by the great current as the resistance of most batteries is very small. The thermal runaway may even be aroused for lithium-ion batteries by short circuit, that both heat and temperature are kept increased to ultimately lead battery packs to explode. In general, a lot of voltage sources, e.g., battery charger, backup power source, and grid-connected generators, can only be paralleled after special protection design to prevent such mismatch damages. Different from these voltage sources, mismatched TEMs do not have the charging and security risks in the case of parallel connection. Consequently, series and parallel connection are of equal importance in composing TEM arrays to satisfy the technical tradeoff between the reliability and the power generation specifications imposed by the practical load voltage and current.

Yet a well recognized rule in designing such a series/parallel hybrid battery pack as TEM arrays is that every cell should have close electric parameters in order to make the power loss caused by the mismatch minimal [20]. The electric parameters refer to the open-circuit voltage and the internal resistance for Thevenin's voltage sources. As the TEMs connected together are usually represented by Thevenin's voltage source model, they should ideally be of similar voltage and resistance characteristics to each other so that no degraded battery limits the string current or the total voltage. However, both theoretical [1–4,6,7,9,11,12,16,18] and

* Corresponding author.
E-mail address: chenminmike@gmail.com (M. Chen).

http://dx.doi.org/10.1016/j.energy.2014.10.021
0360-5442/

experimental [5,8,10,13–15,17,19] investigations clearly show that the variance of the temperature difference applying to different TEMs in most thermal systems can be as much as a few hundred degrees. Since the voltage as well as the internal resistance of a TEM are nonlinearly determined by its hot and cold temperatures, the TEM mismatch power loss is inherently associated with most TEM arrays.

As can be proven in terms of the fundamental circuit theory and shown by means of numerical calculation [3,7,11] and experiment test [21], the maximum power capability of a TEM array, measured by the ratio between its equivalent open-circuit voltage and equivalent internal resistance, may be lowered by the inclusion of some TEMs with smaller temperature difference due to the mismatch power loss. In this case, however, the possibility to optimize the array output power by the removal of the TEMs operating with lower heat source temperature, implemented by replacing the traditionally fixed hardwire interconnections between the TEMs with controllable switches, has only received some attention recently [22]. Once the array is spitted into two sub-arrays, and one can be assumed as the original array whilst the other is composed of the removed TEMs, it is also possible to configure each of the sub-arrays with an individual power electronics stage and MPPT (maximum power point tracking) controller [23]. In this way, not only the mismatch power loss caused by the temperature nonuniformity is recovered, but more power may also be produced than the original TEM array with uniform temperature distribution and zero power loss.

From the practical viewpoint, it is thus important to both qualitatively and quantitatively evaluate how small the temperature difference of certain TEMs is enough that their disconnection from the array would be beneficial. The issue has not been thoroughly covered by the previous works focusing on the controller design and implementation [22,23], but can be identified in an alternative way to find out the extremum of the maximum output power for a TEM array with various temperature distribution patterns. Such a power maximum determines the best occasion to optimally remove TEMs/split the array, and is corresponding to the so-defined critical power point. The main objective of this paper is to carry out the qualitative and quantitative evaluation mentioned above, and the diagnoses of the critical power point will be realized by means of the analytical, experimental, and numerical approaches, respectively, aiming for the feasible design assistance and guide in building practical TEG systems. The main contribution of the analytical study is to rigorously analyze the mismatch power loss in TEGs and formulate the critical power point to optimally split TEM arrays in terms of both series connection and parallel connection (Section 2). The main contribution of the experiments, taken from a practical TEG consisting of eight independently controlled TEMs, is to confirm the theories of critical power point and provide concrete figures on the magnitude of thermal imbalance to arise such critical power points (Section 3). The main contribution of the thermo-electro coupled simulation, using the hierarchical TEG modeling in the circuit simulator SPICE as the ideal solution, is to accurately predict TEG behaviors at the system level, where multiple TEMs can be both electrically connected and thermally combined arbitrarily (Section 4).

2. Mismatch power loss and critical power point

A common configuration to create the temperature difference for a TEG is the fluid-to-fluid heat transfer, where a number of TEMs are placed in the heat exchanger interface separating a hot fluid stream and a cold fluid stream, and generate power as the heat flows through them [1–4,7,10–14,19]. Each TEM is electrically described as a voltage source serially connected with a resistor [24], and when all TEMs are connected in series, the total voltage and resistance of the TEG in the quasi-one dimensional (1D) configuration [25] can be described as.

$$V=\sum_{i=1}^{L_f/w} N\left(\int_{T_c(i)}^{T_h(i)} \alpha_p dT_p-\int_{T_c(i)}^{T_h(i)} \alpha_n dT_n\right), \tag{1}$$

$$R=\sum_{i=1}^{L_f/w} N\left(\int_{0(i)}^{L(i)} \frac{\rho_p}{S_p}dx+\int_{0(i)}^{L(i)} \frac{\rho_n}{S_n}dx\right). \tag{2}$$

As shown in Eqs. (1) and (2), the local power generation of any TEM in the TEG system can be developed by the nonlinear integral functions within the local temperature difference, i.e., from $T_c(i)$/$0(i)$ to $T_h(i)$/$L(i)$, where heat source temperatures T_h and T_c can be assumed same for all thermocouples of each individual TEM. The power capability of the TEG with all TEMs connected together is described as.

$$P=\frac{V^2R_l}{(R+R_l)^2}, \tag{3}$$

which is maximized when $R_l=R$, i.e.,

$$P_{max}=\frac{V^2}{4R}. \tag{4}$$

Similarly, when all TEMs are connected in parallel, V and R of the TEG can be described as.

$$V=\frac{\sum_{i=1}^{L_f/w}\frac{N\left(\int_{T_c(i)}^{T_h(i)} \alpha_p dT_p-\int_{T_c(i)}^{T_h(i)} \alpha_n dT_n\right)}{N\left(\int_{0(i)}^{L(i)} \frac{\rho_p}{S_p}dx+\int_{0(i)}^{L(i)} \frac{\rho_n}{S_n}dx\right)}}{\sum_{i=1}^{L_f/w}\frac{1}{N\left(\int_{0(i)}^{L(i)} \frac{\rho_p}{S_p}dx+\int_{0(i)}^{L(i)} \frac{\rho_n}{S_n}dx\right)}}, \tag{5}$$

$$R=\frac{1}{\sum_{i=1}^{L_f/w}\frac{1}{N\left(\int_{0(i)}^{L(i)} \frac{\rho_p}{S_p}dx+\int_{0(i)}^{L(i)} \frac{\rho_n}{S_n}dx\right)}}. \tag{6}$$

According to Kirchhoff circuit laws, the numerator of Eq. (5) represents the sum of the ratios between the voltage and the resistance of all TEMs, i.e., $\sum V_i/R_i$, and the denominator of Eqs. (5) and (6) represents the sum of the reciprocals of the resistance of all TEMs, i.e., $\sum 1/R_i$. Although all TEMs are connected in parallel, the N pairs of thermoelements within each TEM are usually connected in series, as shown in (5) and (6).

Other instances of TEG heat source include various waste-heat recovery applications in the outer walls of exhaust pipes or combustors [5,6,8,15–18]. When all TEMs are connected in series, the total voltage and resistance of the TEG in the two-dimensional (2D) configuration can be similarly described as.

Please cite this article in press as: Chen M, Gao X, Theoretical, experimental and numerical diagnose of critical power point of thermoelectric generators, Energy (2014), http://dx.doi.org/10.1016/j.energy.2014.10.021

$$V = \sum_{i=1}^{D_w/S} N\left(\int_{T_c(i)}^{T_h(i)} \alpha_p dT_p - \int_{T_c(i)}^{T_h(i)} \alpha_n dT_n\right), \quad (7)$$

$$R = \sum_{i=1}^{D_w/S} N\left(\int_{0(i)}^{L(i)} \frac{\rho_p}{S_p} dx + \int_{0(i)}^{L(i)} \frac{\rho_n}{S_n} dx\right), \quad (8)$$

and when all TEMs are connected in parallel,

$$V = \frac{N\left(\int_{T_c(i)}^{T_h(i)} \alpha_p dT_p - \int_{T_c(i)}^{T_h(i)} \alpha_n dT_n\right)}{\sum_{i=1}^{D_w/S} \frac{N\left(\int_{0(i)}^{L(i)} \frac{\rho_p}{S_p} dx + \int_{0(i)}^{L(i)} \frac{\rho_n}{S_n} dx\right)}{1}}, \quad (9)$$

$$R = \frac{1}{\sum_{i=1}^{D_w/S} \frac{1}{N\left(\int_{0(i)}^{L(i)} \frac{\rho_p}{S_p} dx + \int_{0(i)}^{L(i)} \frac{\rho_n}{S_n} dx\right)}}. \quad (10)$$

Eqs. (3) and (4) can still be applied to obtain the power output in the 2D case.

The circuit of the series connected TEMs, described by Eqs. (1), (2), (7) and (8), can also be generally visualized by Fig. 1 (a), in which M may be equal to $\lfloor L_f/w \rfloor$ or $\lfloor D_w/S \rfloor$ for the 1D or the 2D case, respectively. The voltage source V_j composed by the dotted line represents the depressed TEM subjected to a small ΔT_j. If V_j is idealized that its resistance $R_j = 0$, the power output of the remaining TEMs in the circuit system will not be affected irrespective of how small V_j is. Nevertheless, practical TEMs always exhibit an internal resistance that in this way R_j will lower the power capability of other high voltage TEMs, and may even cause the TEM string with V_j to deliver less power to the load than the remaining TEMs without V_j.

In order to investigate the condition for such a critical power point, e.g., how small V_j or how big R_j is, it is necessary to rigorously formulate the power loss caused by the mismatch among the TEMs connected together. By reducing Eqs. (1), (2), (7), (8) and

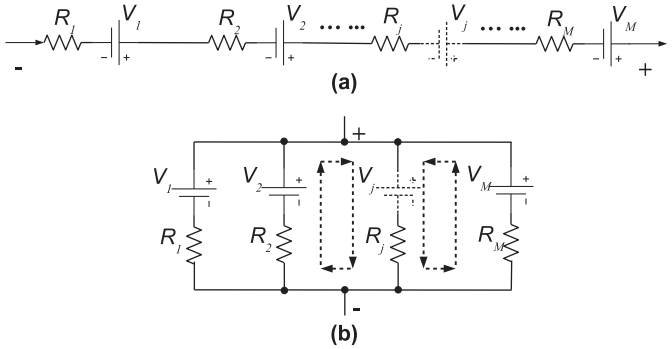

Fig. 1. Power source pack with TEM cells. (a) Series connection model. (b) Parallel connection model.

substituting them into Eq. (4), the comparison between the TEG P_{max} and the sum of P_{max} of all TEMs yields.

$$P_{max} - \sum_{i=1}^{M} P_{max\,i} = \frac{\left(\sum_{i=1}^{M} V_i\right)^2}{4\sum_{i=1}^{M} R_i} - \sum_{i=1}^{M} \frac{V_i^2}{4R_i} = \frac{\left(\sum_{i=1}^{M} \frac{V_i}{2\sqrt{R_i}} 2\sqrt{R_i}\right)^2}{\sum_{i=1}^{M}\left(2\sqrt{R_i}\right)^2} - \sum_{i=1}^{M}\left(\frac{V_i}{2\sqrt{R_i}}\right)^2 \le 0. \quad (11)$$

According to Cauchy inequality, Eq. (11) is equal to zero only if $V_1/R_1 = V_2/R_2 = \ldots = V_j/R_j = \ldots = V_M/R_M$, which means that the TEG P_{max} is equal to the sum of P_{max} of all TEMs when they generate individually; otherwise $P_{max} < \sum_{i=1}^{M} P_{max\,i}$, and the difference between them is the mismatch power loss occurring inside the TEG. Considering the simplest circuit of two TEMs, if both $V_1 \neq V_2$ and $R_1 \neq R_2$, in principle $V_1/R_1 = V_2/R_2$ is still possible that the equality holds in Eq. (11). However, according to Eqs. (1), (2), (7) and (8) as well as the temperature dependencies of $\alpha_{p,n}$ and $\rho_{p,n}$ of Bismuth Telluride [26], the mostly commercialized thermoelectric material, $R_{1,2}$ will increase when the $\Delta T_{1,2}$ becomes lower but $V_{1,2}$ will decrease for the same change. The condition $V_1/R_1 = V_2/R_2$ to allow such a lossless mismatch is consequently of little probability to appear, not to say the practical series connection with more TEMs. Thus, a TEG without any power loss usually consists of matched TEMs with the same V and R due to the same ΔT; if the TEMs in a series connection are mismatched due to the nonuniform temperature distribution, there is usually a power loss.

If the TEG in Fig. 1(a) cuts off the low voltage TEM V_j and other cells in the TEM string operate with identical ΔT, then P_{max} becomes equal to the power sum of all the remaining individual TEMs because there is no mismatch power loss. The condition for the critical power point can be written as.

$$\left(\sum_{i=1}^{M} \frac{V_i^2}{4R_i} - \frac{V_j^2}{4R_j}\right) - \frac{\left(\sum_{i=1}^{M} V_i\right)^2}{4\sum_{i=1}^{M} R_i} \ge 0, \quad (12)$$

where the terms within the parenthesis amounts to the new P_{max} without V_j. Eq. (12) can be more clearly represented as

$$\sum_{i=1}^{M} \frac{V_i^2}{4R_i} - \frac{\left(\sum_{i=1}^{M} V_i\right)^2}{4\sum_{i=1}^{M} R_i} \ge \frac{V_j^2}{4R_j}, \quad (13)$$

where the left side is simply the mismatch power loss introduced by Eq. (11). Therefore, when TEM V_j is shorted, although the TEG terminal voltage would be lowered, the thermal battery pack may perform better as the power loss caused by the weakest cell in the pack is greater than its power contribution.

Similarly, the circuit of TEMs connected in parallel as well as the depressed TEM V_j due to the non-uniform temperature distribution is shown in Fig. 1(b). The identical end voltage of the paralleled TEMs and their built-in Seebeck-voltage imbalance will lead to a certain amount of power loss, that the TEMs with different potentials waste a part of their work to counteract against each other. The counteracting phenomenon is particularly obvious when the load is in open circuit and no power can be extracted, where there will still be a loop current internally flowing through the TEMs, as shown in Fig. 1(b). Because V_j is less than the voltage of other TEMs, the loop current flows from its anode to its cathode, but flows oppositely from the cathodes to the anodes in the remaining TEMs. In the same way, the branches of each paralleled segment will have

Please cite this article in press as: Chen M, Gao X, Theoretical, experimental and numerical diagnose of critical power point of thermoelectric generators, Energy (2014), http://dx.doi.org/10.1016/j.energy.2014.10.021

different currents in the case of a closed load. Such phenomena within the power source caused by the ΔT mismatch among the parallel TEMs will decrease the power performance, as the TEM V_j partly performs as a load for the power source, decreasing the loading capability of the overall TEG.

The power loss caused by the mismatch among the TEMs connected in parallel can be obtained by reducing Eqs. (5), (6), (9), (10) and substituting them into Eq. (4).

$$P_{\max} - \sum_{i=1}^{M} P_{\max\, i} = \frac{\left(\sum_{i=1}^{M} \frac{V_i}{R_i}\right)^2}{4\sum_{i=1}^{M} \frac{1}{R_i}} - \sum_{i=1}^{M} \frac{V_i^2}{4R_i}$$
$$= \frac{\left(\sum_{i=1}^{M} \frac{V_i}{2\sqrt{R_i}} \frac{2}{\sqrt{R_i}}\right)^2}{\sum_{i=1}^{M} \left(\frac{2}{\sqrt{R_i}}\right)^2} - \sum_{i=1}^{M} \left(\frac{V_i}{2\sqrt{R_i}}\right)^2 \le 0. \quad (14)$$

By applying the Cauchy inequality theory again, Eq. (14) is equal to zero only if $V_1 = V_2 = \ldots = V_j = \ldots = V_M$, where the TEG $P_{\max}$ is equal to the sum of the individual $P_{\max}$ of all TEMs and there is no mismatch power loss; otherwise $P_{\max} < \sum_{i=1}^{M} P_{\max\, i}$, and the difference between them is the mismatch power loss occurring inside the TEG. If the TEG in Fig. 1(b) cuts off the TEM V_j and other TEMs operate with identical ΔT, $P_{\max}$ becomes equal to the power sum of all the remaining individual TEMs. The condition for the critical power point of the parallelly connected TEMs can be written as.

$$\left(\sum_{i=1}^{M} \frac{V_i^2}{4R_i} - \frac{V_j^2}{4R_j}\right) - \frac{\left(\sum_{i=1}^{M} \frac{V_i}{R_i}\right)^2}{4\sum_{i=1}^{M} \frac{1}{R_i}} \ge 0, \quad (15)$$

where the terms within the parenthesis amounts to the new $P_{\max}$ without V_j. In terms of V_j and R_j, the critical condition can also be written as

$$\sum_{i=1}^{M} \frac{V_i^2}{4R_i} - \frac{\left(\sum_{i=1}^{M} \frac{V_i}{R_i}\right)^2}{4\sum_{i=1}^{M} \frac{1}{R_i}} \ge \frac{V_j^2}{4R_j}, \quad (16)$$

where the left side is the mismatch power loss when the branch of TEM V_j is not open.

The previous works [3,7,11,21] have validated the critical power point of the TEMs connected in series by means of numerical calculation and experiment test. In terms of the above formulation, $P_{\max}$ of the TEMs connected in parallel has the same characteristics as the series connection, as long as the conditions of Eqs. (13) and (16) are met. In Fig. 2, the ΔT of all connected TEMs are sorted as

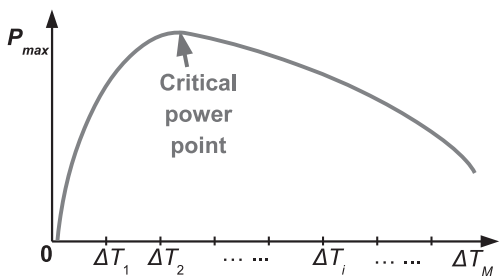

Fig. 2. General characteristics of the TEG critical power point. $\Delta T_1 > \Delta T_2 > \ldots > \Delta T_i > \ldots > \Delta T_M$.

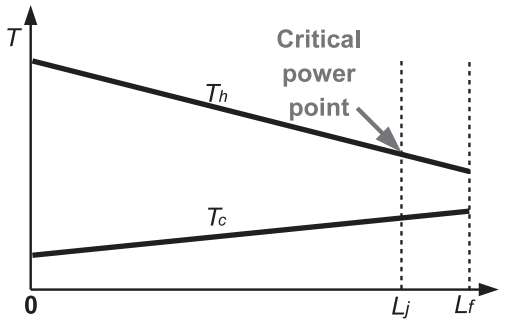

Fig. 3. Temperature profile of the hot and cold fluids with parallel heat exchange and the TEG critical power point.

the horizontal axis, whilst $P_{\max}$ becomes a function of the number of connected TEMs corresponding to the horizontal position. The TEMs in the right side of the critical (peak) power point can be regarded merged as V_j in Fig. 1 as well as (13) and (16) according to the equivalent circuit theorem. Obviously, $P_{\max}$ does not monotonically increase with the increase of the connected TEMs, and in the right side of the critical power point, the more TEMs with small ΔT are connected in the TEG, the less power can be obtained because the increase of the equivalent R_j overwhelms the limited increase of V_j.

For a TEG with the aforementioned quasi-one 1D heat exchange configuration, the critical power point can be defined as either the position of a TEM, as indicated by L_j in Fig. 3, or the ΔT of the TEM at L_j. From 0 to L_j, T_h keeps decreasing and T_c keeps increasing that after L_j the temperature difference will be too small for TEMs to positively generate. If the fluid length is fixed, and from 0 to L_f, T_h keeps decreasing and T_c keeps increasing, the temperature difference distribution between them will be shown as the nearly linear profiles in Fig. 4. The critical power point can be defined as the slope of one of these profiles, where the TEM at L_f has zero contribution to the TEG power output. More nonuniform temperature distributions of ΔT will make one or more TEMs around L_f to become depressed. In this case, the critical power point can also be defined as the actual value of $\Delta T(j)$ at the position L_f, below which the temperature difference will be too small for TEMs to positively generate. For the 2D TEG, the critical power point can be defined alike as the ΔT of the TEM at the 2D position (m,j) in Fig. 5, where darker bars represent depressed TEMs with ΔT coinciding or smaller than the critical power point. Thus, the TEG critical power point with arbitrary temperature distribution can be generalized as the ΔT of a specific TEM position, as shown in Fig. 2. When the mismatch power loss is great enough to enable the occurrence of a critical power point, the disconnection of one TEM or a certain

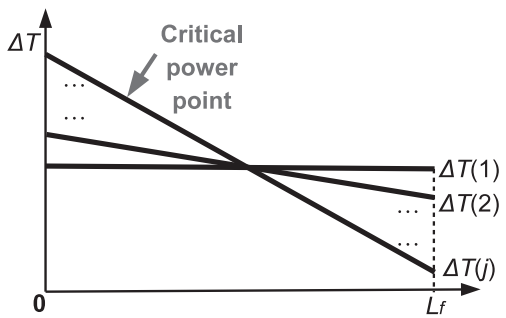

Fig. 4. Temperature difference profiles between the hot and cold fluids with various slopes and the TEG critical power point.

Please cite this article in press as: Chen M, Gao X, Theoretical, experimental and numerical diagnose of critical power point of thermoelectric generators, Energy (2014), http://dx.doi.org/10.1016/j.energy.2014.10.021

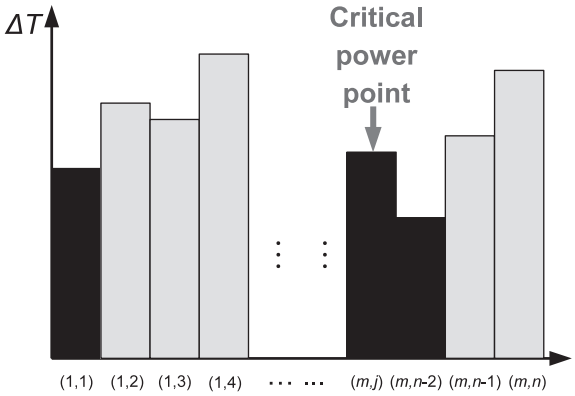

Fig. 5. 2D temperature difference profile and the TEG critical power point.

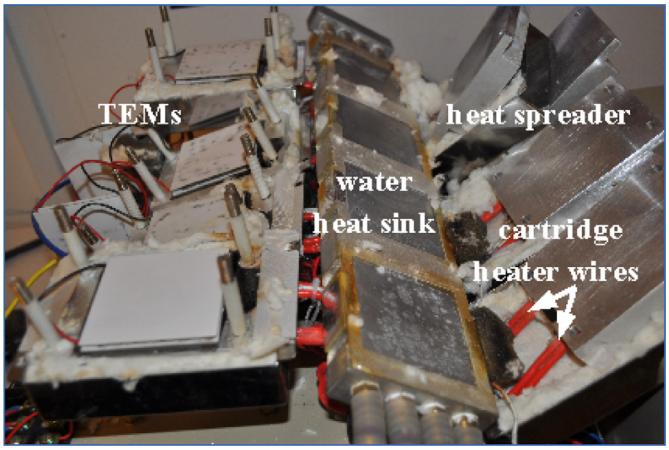

Fig. 7. Illustration of the TEG with setup disassembly.

number of TEMs with ΔT lower than the critical point will be favorable to the overall TEG P_{max}.

3. Experimental diagnose for a practical TEG

In order to characterize TEMs in various interconnection and temperature configurations, the testing apparatus shown in Fig. 6(a1) and Fig. 7 is able to independently control the temperature difference across each of the eight TEMs by eight independent electric heaters. All the data were obtained using TEM devices by Fuxin Co. (TEG1-49-4.5-2.0-250). Each TEM is sandwiched between a hot aluminum heat extender and the cold circulation water chiller, all of which are defined as a TEM unit. In every TEM unit, high power heating elements are embedded in the extender together with thermocouple sensors, and in this way precise temperature measurements are fed back to temperature controllers to automatically fit heater temperatures (T_h) towards the desired values for the TEMs. Thus, the temperature mismatch pattern on the TEM array can be arbitrarily simulated. Any parallel/serial connection of the TEMs can also be implemented at the same time by combining the cell minus/plus lead wires but using the identical stack size.

Given the good flexibility of the rig to enable the TEG to attain the required voltage and current for the load, the 2 × 4 parallel–serial hybrid TEM matrix, as delineated in Fig. 6(a2), is actually connected to the load circuit in the experiments. A minimal boost DC–DC converter prototype is drawn in Fig. 6(a2) to represent the power electric stage part in the load circuit, whilst the full boost power electric schematics actually used can be found in Ref. [27]. The testing results of the hybrid matrix configuration are more

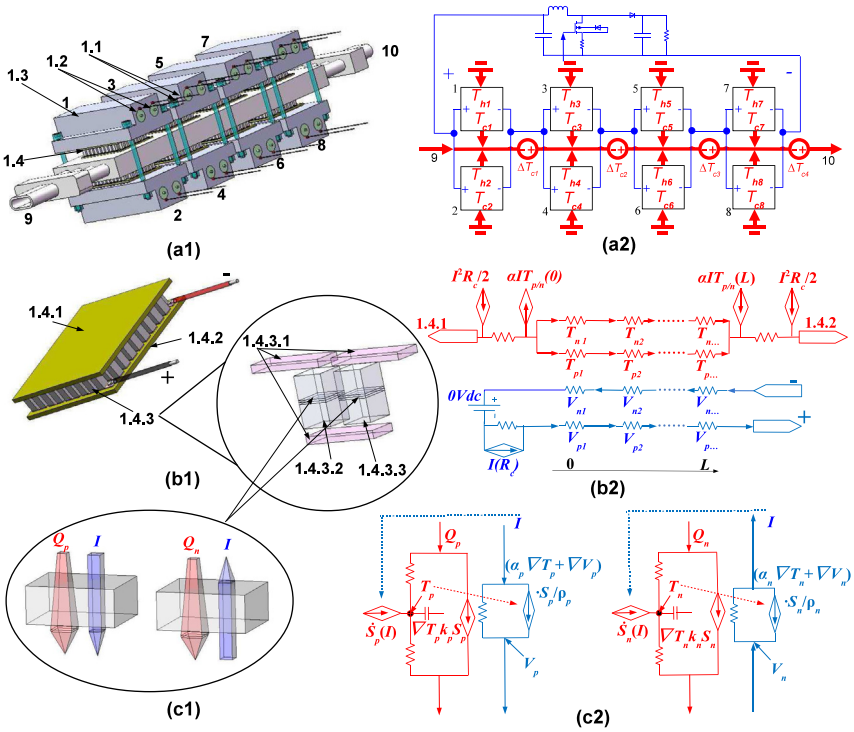

Fig. 6. Experimental and thermal-electric coupled modeling architecture. (a1) TEG test rig. (a2) Hierarchical SPICE modeling at the system level. (b1) TEM_1 and thermocouple closeup. (b2) Lumped SPICE modeling at the TEM level. (c1) Control volume of the p-type and n-type thermoelements. (c2) SPICE modeling of the nonlinear constitutive equations of thermoelectricity.

Please cite this article in press as: Chen M, Gao X, Theoretical, experimental and numerical diagnose of critical power point of thermoelectric generators, Energy (2014), http://dx.doi.org/10.1016/j.energy.2014.10.021

representative and generic than the pure parallel and serial connections of TEM arrays because the latter characteristics are included in the former as its subset.

The accurate characterization of the TEG critical power point is firstly obtained by sweeping $T_{h1,3,5,7}$ from 220 °C down to 80 °C, whilst $T_{h2,4,6,8}$ are kept constant at 220 °C. That is, the initially uniform T_h distribution on the 2 × 4 TEG was changed to be nonuniform, where one half TEMs of the parallel rows are subjected to lower temperature than the other half. Owing to the symmetric structure, the four paralleled TEM pairs in the series circuit are of nearly identical thermal conditions, and hence the power loss within the mismatched parallel rows is mainly examined.

Fig. 8 shows the TEG power change with $T_{h1,3,5,7}$ under various resistive loads. The output of the TEG can also be connected to the electronic load through a DC–DC converter with the traditional MPPT function [27], and the corresponding results are presented by the curve labeled as MPPT mode, where the equivalent resistance of the load circuit automatically coincides the TEG internal resistance by adaptively modulating the duty cycle of the DC–DC converter.

The horizontals in Fig. 8, labeled with "half" and corresponding to various load modes in the figure legend, represent the half value of the initial TEG output power which was achieved under the maximum T_h for all TEMs (220 °C). Any point of intersection between a curve and its counterpart horizontal with the same load, marked by the circles in Fig. 8, represents the critical power point under this load. The value of $T_{h1,3,5,7}$ at this point indicates that ΔT for $TEM_{1,3,5,7}$ has been small enough that the disconnection of them would be advantageous to the TEG power because $TEM_{2,4,6,8}$ themselves along are now able to produce the same amount of power according to the power value tested under the initially uniform T_h. If $T_{h1,3,5,7}$ further decreases that ΔT for $TEM_{1,3,5,7}$ is smaller than the critical power point, more than 50% of original power will be lost even half TEMs ($TEM_{2,4,6,8}$) are still provided with the high temperature 220 °C.

Without changing the electrical connection inside the TEG, the second characterization of the TEG critical power point is obtained by sweeping $T_{h1,2,3,4}$ from 220 °C down to 80 °C, whilst $T_{h5,6,7,8}$ are kept constant at 220 °C. In this case, whether it is a high temperature or a low temperature, the two paralleled TEMs are provided with an identical T_h within any of the four TEM pairs. Thus, the mismatch power loss of the TEM string is mainly examined. Compared with Fig. 8, the critical power points under different load modes in Fig. 9 correspond slightly different values of $T_{h1,2,3,4}$, but they are still closely around 90 °C. In both Figs. 8 and 9, the output power under the MPPT mode is not always greater than other fixed load modes due to the limited optimal operation range of the converter [27], i.e., the power consumption of the converter makes

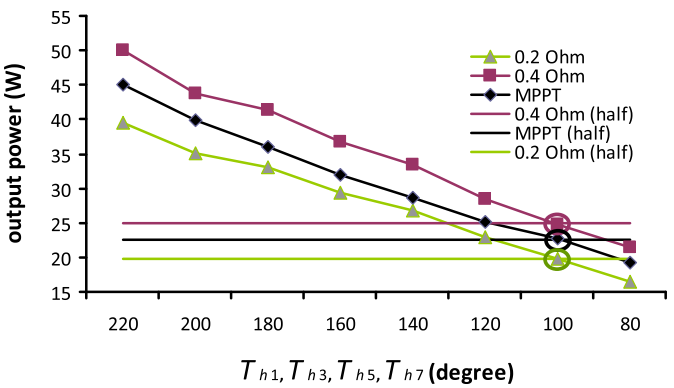

Fig. 8. Output power and critical points of the matrix with eight TEMs under mismatched temperature difference. Load condition is specified in legends.

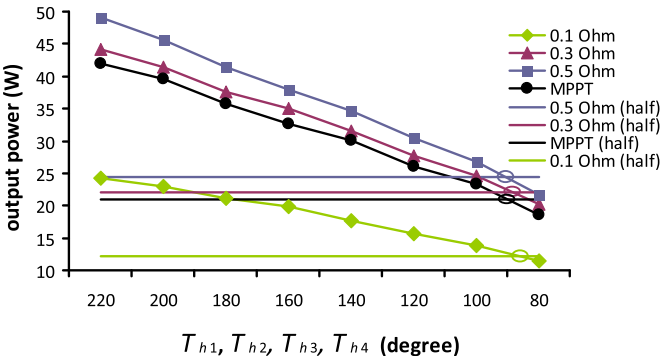

Fig. 9. Output power and critical points of the matrix with eight TEMs under mismatched temperature difference. Load condition is specified in legends.

some fixed loads, when close to the maximum power point, receiving more output of the TEG power than the MPPT mode. The critical power point characteristics are not affected under the MPPT mode though, and it is validated again that 50% power is lost when half TEMs ($TEM_{1,2,3,4}$) are provided with a ΔT equal to the critical power point.

Although the eight TEMs composing the TEG are of the same model, we note that they display heterogeneous electrical performance which also affects the mismatch power loss and the critical power point. One reason is that these TEMs underwent different generation usages (temperature, current, moisture, and compressive load) since the TEG setup had been built. More importantly, the manufacturing tolerance of low cost TEMs such as TEG1-49-4.5-2.0-250 can lead to different aging rates amongst TEMs [22]. The both factors are typical uncertainties that exist in practical industrial TEGs nowadays, which make the accurate prediction by physical simulation difficult. Including the uneven aging of TEMs, however, the experimental results reported above still clearly verify the theories derived in Sec.2 that the critical power point will occur when the temperature mismatch arrives at a certain extent.

4. Generic numerical diagnose by SPICE modeling

With the rapid development of thermoelectric device engineering and TEG installation standardization, more and more high end TEMs are being used with nearly identical aging rates. For the new generation TEG, an accurate and systematic TEG model is necessary to be available for the designer to determine the critical power point under the dynamically changing heat source temperature distribution. The modeling technique based upon the fundamental thermoelectric physical processes can also provide a reference for low cost TEGs using TEMs with heterogeneous electrical parameters if the mismatch power loss is great enough, despite that the actual critical power point of the TEG system consisting of TEMs with mismatched properties may be moderately different from the modeling result.

The theoretical analyses on the critical power point in Sec.2 are formulated and generalized for any number of connected TEMs. It is yet mathematically unrealistic to directly apply Eqs. (13) and (16) due to the nonlinearities presented within Eqs. (1), (2), (7) and (8) and (5), (6), (9), (10), the arbitrary series–parallel-hybrid interconnection of practical TEGs, and the great many TEM interconnection combinations corresponding to various critical power point definitions. In practical control of a partially underheated TEM array caused by the dynamically changing pattern of the temperature profile, both the fixed TEMs and the flexible TEMs for appropriate removal/revival are multiple. In fact, the accurate performance analysis of multiple TEMs has been identified as a

Please cite this article in press as: Chen M, Gao X, Theoretical, experimental and numerical diagnose of critical power point of thermoelectric generators, Energy (2014), http://dx.doi.org/10.1016/j.energy.2014.10.021

main technical issue [21], and a computer model is indeed mandatory to numerically determine the TEG critical power point for each TEM connection combination.

Moreover, a model-based algorithm is also important in adaptively perceiving the optimal array configuration with the maximum output power in terms of the critical power point, that is, when the optimal configuration is executed, underheated TEMs without which the TEGS can output more power can be automatically removed, and removed TEMs can also be automatically revived if their previous low temperature becomes high enough. Such an implementation is described in Ref. [28]: when any switch is open, its relevant TEM will be removed and independent from the array, whilst the removed TEM can also be reconnected into the array if the open switch becomes closed. When the temperature distribution of the heat source is nearly uniform, for instance, the modeless trial and error method is particularly harmful to the generation performance as the continuous trial removal of certain TEMs will lower the output even the removed TEMs can be revived later on. However, the undesirable oscillation and loss on P_{max} can be eliminated by the model-based algorithm with the cost of using sensors.

Therefore, it is important to carefully select the type of sensors in terms of both technical and economical factors in order to fully take the advantages of the model-based algorithm. Voltage and current sensors can be used in terms of the principles formulated in Sec.2 and a pure circuit network model, but the direct measurement of V and R of a TEM in the array is inconvenient and may cause oscillation on P_{max}. The influences of the thermal-electric coupled multiphysics effects cannot be included either because the TEM currents during the measurement are likely different from the real values in the actually operating array, leading to some errors of V and R to be input into the electrical model [29]. In effect, Eqs. (1), (2), (7) and (8) and (5), (6), (9), (10) clearly indicate that V and R can also be indirectly computed by means of temperature sensors only through an electrothermal modeling approach such as the one in Refs. [24,25]. By establishing the accurate mapping relation between the heat source temperature distribution and the TEG power performance, the model-based algorithm can still decrease the cost brought by sophisticated sensors as well as the DAQ (data acquisition) to a large extent. Table 1.

Using the temperature input as the boundary condition, an ideal TEG model to be used in the determination of the critical power point and the model-based control algorithm should have the following properties:

1) The model is based on the physical approach and the universal thermoelectric conversion principles rather than the empirical approach from the limited existing data.
2) The temperature dependencies of $\alpha_{p,n}$, $\rho_{p,n}$, and $k_{p,n}$ of the thermoelectric materials are included.
3) The multiphysics coupled effects between the thermal field and the electric field are included.
4) The ability to analyze P_{max} of various series/parallel interconnections of TEMs with different temperature boundaries (and hence different V and R), together with their power electronics stages.
5) A user-friendly design environment.

Table 1
Definition of components in Fig. 6.

Number	Definition
1–8	TEM units 1–8
9	Coolant inlet
10	Coolant outlet
1.1	Temperature sensors of the TEM unit
1.2	Cartridge heating rods
1.3	Aluminum heat extender
1.4	TEM_1
1.4.1	Top ceramic layer
1.4.2	Bottom ceramic layer
1.4.3	Thermoelements
1.4.3.1	Conducting bridges
1.4.3.2	p-type leg
1.4.3.3	n-type leg

The electrothermal model in Ref. [24] is based on the full physical details and nonlinear constitutive equations of the thermoelectric conversion. Fig. 6(b1) illustrates the schematic of one TEM, i.e., TEM1, whose fundamental generation thermocouple is modeled in Fig. 6(b2), where the potential ($V_{p,n}$) and temperature ($T_{p,n}$) distributions inside the TEM are solved, respectively. Appropriately scaled by N, R_c [30] is simulated in the electric circuit, and its Joule effect is divided uniformly to be simulated in the hot and cold sides of the thermal circuit. The control volume of the thermocouple is depicted in Fig. 6(c1) with the heat and electric fluxes flowing through, whilst its SPICE model is shown in Fig. 6(c2), where both the temperature dependent heat and electricity conductions, as well as the multiphysics coupled effects, are numerically implemented. Based upon electrothermal analogy, the circuit simulator SPICE is used to realize the multiphysics coupled algorithm, where the thermal and electrical simulations are performed in the same modeling tool. As shown in Fig. 6(b2) and (c2), between the isolated thermal and electrical circuits, no additional routine is required to control their information exchange and iteration for the current-related heat source terms, i.e., Peltier, Joule, and Thomson effects, i.e.,

$$\dot{S}_{p,n}(I) = I^2 \frac{\rho_{p,n}(T_{p,n}(x))}{S_{p,n}} dx + \nabla \alpha_{p,n}(T_{p,n}(x)) dx T_{p,n}(x) I, \quad (17)$$

and for the temperature dependent V and R. By the TEM model, the corresponding relationship between the thermal/load boundary condition and the TEM performance parameters (power, efficiency, voltage and resistance) has been elegantly built and experimentally validated [24].

By upgrading the TEM level model to the system level [25], multiple TEMs spatially distributed in the thermal system can freely constitute an array of whatever configuration, including both series connection and parallel connection. The inherent nature of the SPICE circuit simulator also helps the implementation of the cosimulation of the TEM array with its power electronics interface and MPPT controller. In the TEG model, a hierarchical and TEM-object oriented strategy is utilized that each TEM type is defined as a class, in which all detailed simulation procedures and device data of the TEM type are packaged and become invisible to the outside of the class. At the system level, only one TEM class is invoked for all TEM instances of the same type, and every TEM instance only has four input and output (I/O) ports to be manipulated, i.e., T_h, T_c, plus, and minus lead wires, as shown in Fig. 6(a2). In this way, the maintainability, scalability, development efficiency, and execution efficiency of the TEG modeling code is essentially improved [25].

Using the SPICE modeling, the TEG setup described in Sec.3 and Fig. 6(a) is simulated to numerically quantify the characteristics of the critical power point. Firstly a DC sweep analysis on the voltage source emulating T_{h4} is performed to obtain the critical power point of a single low temperature TEM. In Fig. 10, it is noteworthy that the output power is not completely constant when TEM_4 is excluded from the SPICE simulation because the water temperature variation is taken into account at the cold side. As shown in Fig. 6(a2), with

Please cite this article in press as: Chen M, Gao X, Theoretical, experimental and numerical diagnose of critical power point of thermoelectric generators, Energy (2014), http://dx.doi.org/10.1016/j.energy.2014.10.021

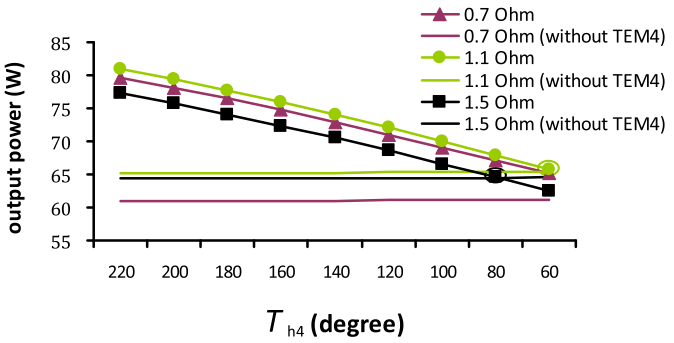

Fig. 10. Output power and critical points of the matrix with TEM_4 under low T_h. $T_{h1-3,5-8} = 220$ °C.

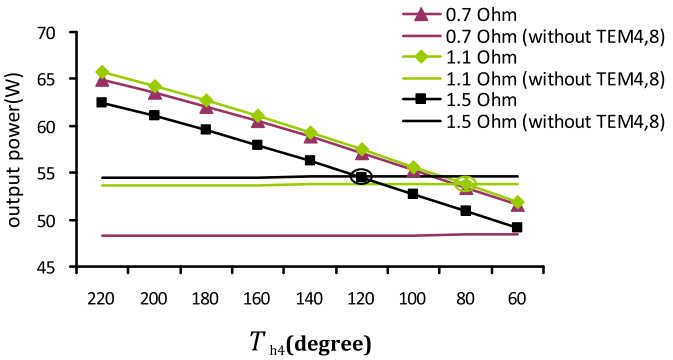

Fig. 12. Output power and critical points of the matrix with $TEM_{4,8}$ under low T_h. $T_{h1-3,5-7} = 220$ °C. $T_{h8} = 60$ °C.

the decrease of T_{h4}, the heat flow added from TEM_4 to the coolant fluid is decreased, too. Consequently, T_c for the downstream TEMs is gradually lowered to furnish these TEMs larger ΔT, and the TEG output power is hence increased.

Fig. 10 shows that the critical power point value of T_{h4} is about 80 °C and 60 °C for $R_l = 1.5\Omega$ and $R_l = 1.1\Omega$, respectively. When $R_l = 0.7\Omega$, the critical power point does not appear within the figure scope, which indicates that ΔT for TEM_4 is still not small enough and the disconnection of it would decrease P. In Fig. 11, T_h of other TEMs is purposely designed to be nonuniform to enhance the testing diversity. However, the critical power point characteristics are nearly identical to Fig. 10 in this case.

The second DC sweep analysis is performed to obtain the critical power point characteristics of two low temperature TEMs, i.e., TEM_4 and TEM_8. In Fig. 12, T_{h8} is fixed at 60 °C, and T_{h4} is decreased from 220 °C down to 60 °C. It is found that the critical power point of T_{h4} is about 120 °C and 80 °C for $R_l = 1.5\Omega$ and $R_l = 1.1\Omega$, respectively, and when $R_l = 0.7\Omega$, the critical power point does not appear within the figure scope. When both T_{h4} and T_{h8} are swept from the high temperature to the low temperature, the critical power point is about 75 °C and 60 °C for $R_l = 1.5\Omega$ and $R_l = 1.1\Omega$, and again, the critical power point does not appear when $R_l = 0.7\Omega$, as shown in Fig. 13.

5. Conclusions

The optimization approach in terms of the critical power points is an extremely important research topic in the development of TEG applications. Such an optimization can reduce the negative effects of the temperature mismatch on the output power, which has been commonly observed by TEG system designers, and hence considerably increase the actual energy efficiency of practical TEGs. One key step in making the optimization feasible is to determine the critical power points and quantify their magnitude under various operating conditions. Exploiting the principles of battery mismatch, rigorous analytical derivation is given in this paper on the critical power point. It is mathematically proven that when some TEMs are exposed to a smaller heat source ΔT in a TEM array, the generated TEG power can be more by removing them because of their internal energy consumption. The theoretical conceptions and conditions of the critical power point are illustrated by experiments and numerical simulations of a series–parallel hybrid interconnected TEM matrix, respectively. In experimental and numerical results, a number of critical power points are disclosed for the TEG prototype, where T_h mostly ranges from 120 °C to 60 °C. The experimental results prove themselves that the critical power points for the TEG composed of TEG1-49-4.5-2.0-250 are accurately determined, and critical power points for other systems can be accurately determined by the same approach. More generally, the SPICE simulator is used as the modeling and programming tool and facilitates the maximum-power oriented configuration for live TEGs at large by means of the hierarchical cosimulation approach, where all major thermoelectric nonlinearities, i.e., thermo-electro coupled multiphysics behaviors and temperature dependent material properties, are included. The accuracy of the TEG model has also been verified by many previous experiments [24–26,29], including those on the critical power points [28].

In principle, it is possible that removing certain TEM(s) of higher temperature difference can give more output power than removing certain TEM(s) of lower temperature difference from the same configuration. Such examples are particularly likely to be illustrated when the TEM array is of asymmetric and irregular structure and/or when the TEM array is operating in connection with other power

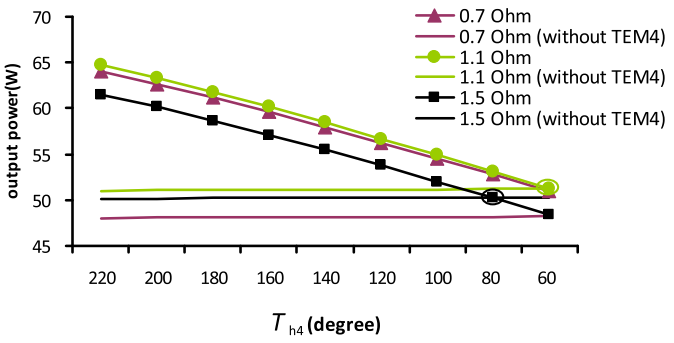

Fig. 11. Output power and critical points of the matrix with TEM_4 under low T_h. $T_{h1-3,5-8} = 220$ °C,210 °C,200 °C,190 °C,180 °C,170 °C,160 °C.

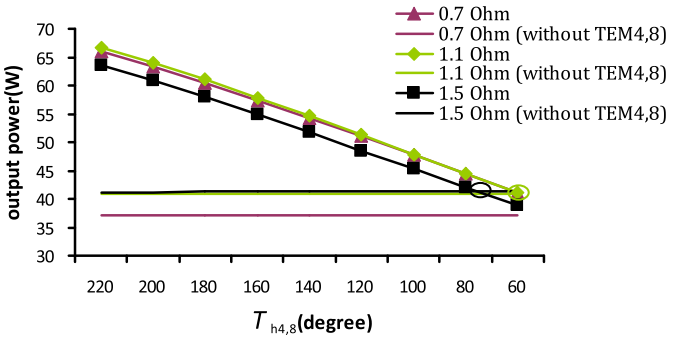

Fig. 13. Output power and critical points of the matrix with $TEM_{4,8}$ under low T_h. $T_{h1-3,5-7} = 220$ °C,210 °C,200 °C,180 °C,170 °C,160 °C.

Please cite this article in press as: Chen M, Gao X, Theoretical, experimental and numerical diagnose of critical power point of thermoelectric generators, Energy (2014), http://dx.doi.org/10.1016/j.energy.2014.10.021

sources such as fuel cells/PV cells/battery packs, where, apart from the temperature, the position of each TEM also matters. In this case, an exhaustive traveling of all possibilities of power increase is the safest way to attain the globally optimal configuration. It is yet important to acknowledge that the conception of critical power point, to search only within those topologies removing underheated TEMs instead of all topologies, is valuable in dealing with common TEGs which are mostly applied in practice. The possibility will also exist to work on a range of problems relating the critical power point to TEG security, as the physically destroyed TEMs may also be adaptively removed so that the performance of the TEG is actually able to self-heal.

Acknowledgments

This work is funded in part by the Danish Council for Independent Research and in part by the Danish Council for Technology and Production Sciences under Grant 09-069739.

Nomenclature

$\dot{S}$	heat source term (W)
D_w	area of the heat source (m^2)
dx	1D control volume length in thermoelements (m)
I	current (A)
i	TEM number
k	thermal conductivities (W/mK)
L	length of the p- and n-type legs (m)
L_f	length of the fluid path (m)
L_j	position of the TEM at the critical power point (m)
M	total number of TEMs in the TEG
m	maximum number of TEMs in the horizontal coordinate of 2D TEG
N	number of pairs of thermoelements in each TEM
n	maximum number of TEMs in the vertical coordinate of 2D TEG
P	power on the load (W)
P_{max}	maximum power (W)
Q	conduction heat flow in p-type or n-type thermoelement (W)
R	internal resistance (Ω)
R_c	contact resistance across conducting bridges
R_l	load resistance (Ω)
S	uniform cross-sectional area of TEM (m^2)
S_n	uniform cross-sectional area of n-type leg (m^2)
S_p	uniform cross-sectional area of p-type leg (m^2)
T	temperature (K)
V	open-circuit electric potential (V)
w	dimension of each TEM in the direction of the fluid flow (m)

Greek symbols

α	Seebeck coefficient, (VK^{-1})
ΔT	temperature difference across the TEM, $T_h - T_c$, (K)
ρ	electrical resistivity (Ω m)

Subscripts

c	cold side
h	hot side
j	TEM number
n	n-type material or leg
p	p-type material or leg

References

[1] Bohn MS. Heat-exchanger effectiveness in thermoelectric power generation. ASME J Heat Transf 1981;103:693–8.
[2] Esarte T, Gao M, Rowe DM. Modelling heat exchangers for thermoelectric generators. J Power Sources 2001;93:72–6.
[3] Suzuki R. Mathematic simulation on power generation by roll cake type of thermoelectric double cylinders. J Power Sources 2004;133:277–85.
[4] Chen M, Lund H, Rosendahl L, Condra T. Energy efficiency analysis and impact evaluation of the application of thermoelectric power cycle to today's CHP systems. Appl Energy 2010;87:1231–8.
[5] Kaibe H, Kajihara T, Fujimoto S, Makino K, Hachiuma H. Recovery of plant waste heat by a thermoelectric generating system. Komatsu Tech Rep 2011;57:26–30.
[6] Chen M, Sasaki Y, Suzuki RO. Computational simulation of thermoelectric generators in marine power plants. Mater Trans 2011;52:1549–52.
[7] Suzuki RO, Sasaki Y, Fujisaka T, Chen M. Effects of fluid directions on heat exchange in thermoelectric generators. In: Proc. 2012 38th conference of the IEEE ind. electron. soc; 2012. p. 5877–82.
[8] Chen M, Andreasen SJ, Rosendahl LA, Kær SK, Condra TJ. System modeling and validation of a thermoelectric fluidic power source – proton exchange membrane fuel cell and thermoelectric generators (PEMFC-TEG). J Electron Mater 2010;39:1593–600.
[9] Chen M, Rosendahl LA, Condra T. A three-dimensional numerical model of thermoelectric generators in fluid power systems. Int J Heat Mass Transf 2011;54:345–55.
[10] Bensaid S, Brignone M, Ziggiotti A, Ziggiotti S. High efficiency thermo-electric power generator. Int J Hydro Energy 2012;37:1385–98.
[11] Gao X, Andreasen SJ, Chen M, Kaer SK. Numerical model of a thermoelectric generator with compact plate-fin heat exchanger for high temperature PEM fuel cell exhaust heat recovery. Int J Hydro Energy 2012;37:8490–8.
[12] Kousksou T, Bedecarrats J, Champier D, Pignolet P, Brillet C. Numerical study of thermoelectric power generation for an helicopter conical nozzle. J Power Sources 2011;196:4026–32.
[13] Kim S, Park S, Kim S, Rhi S. A thermoelectric generator using engine coolant for light-duty internal combustion engine-powered vehicles. J Electron Mater 2011;40:812–6.
[14] Chen W, Liao C, Hung C, Huang W. Experimental study on thermoelectric modules for power generation at various operating conditions. Energy 2012;45:874–81.
[15] Jang JY, Tsai YC. Optimization of thermoelectric generator module spacing and spreader thickness used in a waste heat recovery system. Appl Therm Eng 2013;51:677–89.
[16] Jang JY, Tsai YC, Wu CW. A study of 3-D numerical simulation and comparison with experimental results on turbulent flow of venting flue gas using thermoelectric generator modules and plate fin heat sink. Energy 2013;53:270–81.
[17] Deng YD, Liu X, Chen S, Tong NQ. Thermal optimization of the heat exchanger in an automotive exhaust-based thermoelectric generator. J Electron Mater 2013;42:1634–40.
[18] Roy G, Matagne E, Jacques PJ. A global design approach for large-scale thermoelectric energy harvesting systems. J Electron Mater 2013;42:1781–8.
[19] Favarel C, Bedecarrats JP, Kousksou T, Champier D. Numerical optimization of the occupancy rate of thermoelectric generators to produce the highest electrical power. Energy 2014;68:104–16.
[20] Buchmann I. Serial and parallel battery configurations. 2004 [Online]. Available: www.buchmann.ca.
[21] Gomez M, Ohara B, Reid R, Lee H. Investigation of the effect of electrical current variance on thermoelectric energy harvesting. J Electron Mater 2014;43:1744–51.
[22] Chen M. Distributed detection and control of defective thermoelectric generation modules using sensor nodes. IEEE Trans Instrum Meas 2014;63:192–202.
[23] Wu H, Sun K, Chen M, Xing Y. Hybrid centralized-distributed power conditioning system for thermoelectric generator with high energy efficiency. In: Proc. the IEEE energ. convers. congress. expo; 2013. p. 4659–64.
[24] Chen M, Rosendahl LA, Condra TJ, Pedersen JK. Numerical modeling of thermoelectric generators with varying material properties in a circuit simulator. IEEE Trans Energy Convers 2009;24:112–24.
[25] Chen M, Gao J, Kang Z, Zhang J. Design methodology of large-scale thermoelectric generation: a hierarchical modeling approach. ASME J Therm Sci Eng Appl 2012;4:041003.
[26] Zhu J, Gao J, Chen M, Zhang J, Du Q, Suzuki RO, et al. Experimental study of a thermoelectric generation system. J Electron Mater 2011;40:744–52.
[27] Gao J, Sun K, Ni L, Chen M, Kang Z, Zhang L, et al. A thermoelectric generation system and its power electronics stage. J Electron Mater 2012;41:1043–50.
[28] Chen M. Adaptive removal and revival of underheated thermoelectric generation modules. IEEE Trans Ind Electron 2014;61:6100–7.
[29] Gao J, Chen M. Beat the deviations in estimating maximum power of thermoelectric modules. IEEE Trans Instrum Meas 2013;62:2725–9.
[30] Chen M. Note: extraction of temperature-dependent interfacial resistance of thermoelectric modules. Rev Sci Instrum 2011;82:116109.

Please cite this article in press as: Chen M, Gao X, Theoretical, experimental and numerical diagnose of critical power point of thermoelectric generators, Energy (2014), http://dx.doi.org/10.1016/j.energy.2014.10.021